

Special Issue of the 6th International Congress & Exhibition (APMAS2016), Maslak, Istanbul, Turkey, June 1–3, 2016

# Preparation of SnO<sub>2</sub> Thin Film Nanostructure for CO Gas Sensor Using Ultrasonic Spray Pyrolysis and Chemical Bath Deposition Technique

B. YULIARTO<sup>a,b,\*</sup>, G. GUMILAR<sup>a</sup>, D.W. ZULHENDRI<sup>a</sup>, NUGRAHA<sup>a,b</sup> AND N.L.W. SEPTIANI<sup>a,b</sup>

<sup>a</sup>Advanced Functional Materials Laboratory, Engineering Physics Department, Institut Teknologi Bandung, Bandung, Indonesia

<sup>b</sup>Research Center for Nanosciences and Nanotechnology, Institut Teknologi Bandung, Bandung, Indonesia

In recent years, research of metal oxide semiconductor-based sensors has focused on morphology modification of thin film structures. One of the promising materials that is being developed is SnO<sub>2</sub>. In this research, nanostructured SnO<sub>2</sub> thin film was grown using the ultrasonic spray pyrolysis and chemical bath deposition methods with and without external magnet assistance (0.1 T). As precursor solution of the ultrasonic spray pyrolysis process, the SnCl<sub>2</sub>·2H<sub>2</sub>O is dissolved in distilled water, with pH varied by adding 37% HCl solution. The precursor solution for the chemical bath deposition process was SnCl<sub>2</sub>·2H<sub>2</sub>O, which is dissolved in urea solution with pH customized by adding the NaOH solution. All resulting nanostructured SnO<sub>2</sub> thin film samples were characterized by using X-ray diffraction and scanning electron microscopy techniques. The resulting morphologies of SnO<sub>2</sub>, prepared by chemical bath deposition, using magnetic field, HMTA framework-assisted chemical bath deposition, and ultrasonic spray pyrolysis are spherical, cubic, and spherical, respectively. The sensor response pattern of nanostructured SnO<sub>2</sub> thin films, prepared by all tested methods, to 30 ppm CO, is similar in that the response increases with the increase of working temperature. The SnO<sub>2</sub> thin film prepared by ultrasonic spray pyrolysis method shows the greatest sensitivity value of 95.12%, with a response time of 216 seconds and a recovery time of 558 seconds, at working temperature of 300 degrees Celsius.

DOI: [10.12693/APhysPolA.131.534](https://doi.org/10.12693/APhysPolA.131.534)

PACS/topics: 68.43–h

## 1. Introduction

Recently, in almost all countries around the world, the numbers of vehicles has increased significantly. The majority of vehicles use gasoline or oil as a primary fuel. The incomplete combustion process of fuel produces CO gas that is harmful for our health and the environment. The increasing number of vehicles will increase the total amount of CO gas emission per year. Besides that, the large number of factories also increases the total amount of CO gas emission per year. Therefore, gas monitoring system is highly required to monitor and to reduce the risk of this harmful gas. In air pollution monitoring systems, the gas sensor has a key function in detecting and measuring the concentration of the targeted gas. A promising monitoring gas sensor is a metal oxide semiconductor-based sensor. Among the metal oxide sensors, SnO<sub>2</sub> has been the most studied sensitive layer.

SnO<sub>2</sub> is a typical n-type semiconductor with a wide band gap of 3.6 eV [1–7]. SnO<sub>2</sub> has been identified as a potential semiconductor material with many applications, including acting as a supercapacitor [8], catalyst [9], energy storage [10] and as gas sensor [11]. SnO<sub>2</sub> is preferable and has been investigated by many researchers for gas sensor application because SnO<sub>2</sub> is highly sensitive

to various pollutant gases. The relatively lower working temperature of SnO<sub>2</sub> and higher performance, compared to other metal oxides, make SnO<sub>2</sub> important as a potential high performance gas sensor material. Moreover, the SnO<sub>2</sub>'s stability has led to further studies, aimed at making it perform better and to consume less energy.

Studies show that the morphology, structure and size of metal oxide materials have been proven to influence the sensing performance of SnO<sub>2</sub> [12]. The recent developments of tin dioxide sensors have been focused on the increasing surface area, so that the interaction between targeted gas and the sensitive layer of tin dioxide increases [3]. The more interaction between pollutant gas particles and the surface of the sensitive metal oxide layer, the higher is the sensitivity of the sensor.

One approach to increasing the surface area of the metal oxide is to modify the morphology of the metal oxide surface using the nanostructured pattern. The goal of this surface modification is to control the active surface, because increasing the contact area between material and target gas will provide more surface-active area sites for the sensing reactions. The larger space in the inside part in the nanostructure will provide a better transport channel, so that the gas diffusion of target gas molecules becomes more suitable for gas sensor application [12].

This paper explains the synthesis of SnO<sub>2</sub> thin film nanostructures by two different techniques. The chemical bath deposition (CBD) and ultrasonic spray pyrolysis (USP) methods can be used to yield a different types

\*corresponding author; e-mail: [brian@tf.itb.ac.id](mailto:brian@tf.itb.ac.id)

of nanostructure of SnO<sub>2</sub> thin films. The resulting nanostructured thin films obtained both by chemical bath deposition and ultra spray pyrolysis, have been tested for CO gas detection. The effect of different nano patterns of the nanostructured SnO<sub>2</sub> thin films have been studied and the results indicate that the sample prepared by USP shows the highest sensor response.

## 2. Materials and equipment

SnCl<sub>2</sub>·2H<sub>2</sub>O, hydrochloric acid (HCl), sodium hydroxide (NaOH), urea, and hexamethyl tetra amine (HMTA) were obtained from Merck. All raw materials that were used in this research, including ethanol, acetone, and double distilled water, were analytic reagent grade and were used without any purification.

The schematic synthesis procedure can be seen in the Fig. 1, where the amount of SnCl<sub>2</sub>·2H<sub>2</sub>O was dissolved in double distilled water and was stirred for 30 min. HCl was then added dropwise until the pH of solution reached 1. Then the solution was stirred for another 30 minutes.

The USP process can be explained as follows: the prepared solution was placed in the container and it was ultrasonicated until the droplets formed. The droplets were then compressed until they reached the substrate, which was heated to 500 degrees Celsius.

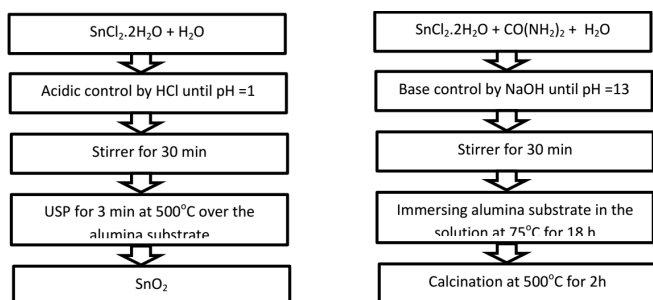


Fig. 1. Flow chart of SnO<sub>2</sub> synthesis process by ultra spray pyrolysis (left) and chemical bath deposition (right).

For CBD, the amount of SnCl<sub>2</sub>·2H<sub>2</sub>O is mixed with urea in double distilled water and was stirred for 30 minutes. NaOH solution was then added dropwise to the solution until the pH reaches 13. Alumina substrate that has been cleaned by ethanol and double distilled water was immersed in the solution at 75 degrees Celsius for 18 hours. After 18 hours of immersion, the SnO<sub>2</sub> thin film formed on the alumina substrate. The resulting sample of the thin film was then rinsed several times with ethanol and water to remove small pollutant particles. Finally, the sample was dried and calcined at 500 degrees Celsius for 2 hours.

In the magnetic field and HMTA framework-assisted CBD, the process of synthesis is similar to CBD, except that the HMTA is added into the solutions before

the base controlled processes. Moreover, the substrate was also immersed in the solution placed over the 0.1 T magnet.

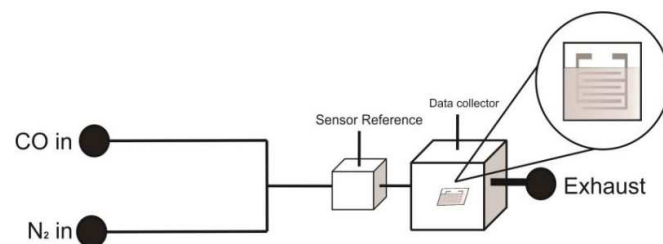


Fig. 2. Illustration of sensor characterization instrument.

The crystal structure of the resulting nanostructured SnO<sub>2</sub> thin films was determined by X-Ray diffraction (XRD) using a Philips Analytical X-Ray with Cu K<sub>α</sub> radiation ( $\lambda = 1.54060 \text{ \AA}$ ) generated at 40 kV and 25 mA. The machine was set to step scan mode with the step size at 0.020 and the step time at 0.5 second for  $2\theta$  interval of 20°–90°.

The morphology of the nanostructured SnO<sub>2</sub> thin films, prepared by both CBD and USP, were observed by scanning electron microscopy (SEM) using JEOL-JSM-6510 LV. Moreover the sensor performance was tested using a sensor system shown in Fig. 2. Figure 2 describes the gas sensor characterization scheme, which is comprised primarily of a CO gas target source, mass flow controller, reference chamber, standard measurement and the test characterization chamber, where the sample was placed. The sensor sample was installed in the test characterization chamber and connected to the voltage unit via data acquisition systems. The sensor response was measured in the presence of CO at various temperatures to find the best operation temperature for the sensor. The N<sub>2</sub> gas was used control the concentration of the CO gas.

## 3. Results and discussion

The diffraction patterns of all nanostructured SnO<sub>2</sub> thin films prepared by USP, CBD, and magnetic field HMTA framework-assisted CBD have similar peaks, as shown in Fig. 3. The peaks of all SnO<sub>2</sub> are relatively sharp, but the sharpest peak comes from the SnO<sub>2</sub> thin film prepared by the USP technique, indicating that the crystallinity of this SnO<sub>2</sub> thin film is better than of the others.

Moreover, all samples of SnO<sub>2</sub> thin films prepared by all methods have a tetragonal rutile crystal structure, which matches with JCPDS card no. 41-1445, where the diffraction planes are (110), (101), (200), and (211). From the XRD characterization, it can be seen, that there is only one phase in the thin films. As a result, there is no other crystal structures or impurities in the resulting SnO<sub>2</sub> thin films.

As the crystallinity is one of the most important parameters, that determines the response of sensors, the good crystallinity of all these resulting nanostructured SnO<sub>2</sub> thin films predicts good potential for gas sensor applications.

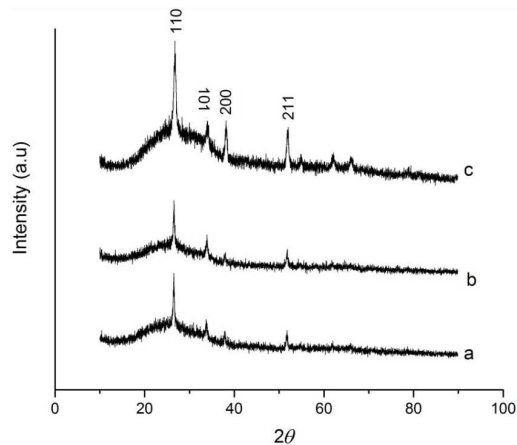


Fig. 3. Diffraction pattern of nanostructured SnO<sub>2</sub> thin films prepared by magnetic and HMTA framework field assisted CBD (a), pure CBD (b), and USP methods (c).

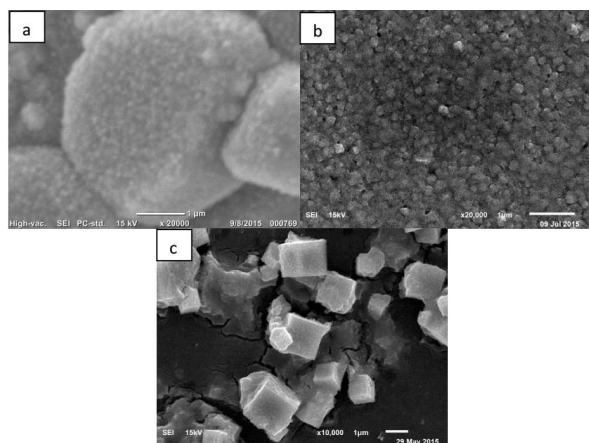


Fig. 4. Various morphologies of nanostructured SnO<sub>2</sub> thin films: spherical shape nanostructure, prepared by USP method (a), spherical shape nanostructure prepared by CBD method (b), and cubic-like pattern prepared by magnetic field and HMTA framework assisted CBD methods (c).

Figure 4 shows different morphologies of SnO<sub>2</sub> thin films, prepared by USP, CBD, and magnetic field HMTA framework-assisted CBD, respectively. The nanostructure of SnO<sub>2</sub> thin films, prepared by the USP method, has a nanoscale spherical shape, with the average features size of about 60 nanometers.

Figure 4a, shows that incomplete agglomeration had occurred where little SnO<sub>2</sub> particles join together with the big particles. In the USP process, droplets of Sn(OH)<sub>4</sub> are generated in the ultra-sonicated solution. The droplets deposited on the heated substrates start to form the thin film.

On the other hand, in Fig. 4b the SnO<sub>2</sub> nanostructures from the CBD method also have spherical shape and a larger size of about 70 nanometers. Unlike the SnO<sub>2</sub> thin film prepared by USP, agglomerations of particles are not visible and the particles are spread evenly over the surface of the substrate in the case of SnO<sub>2</sub> prepared by the CBD method.

Moreover, utilization of magnetic field and HMTA framework in the CBD process yield SnO<sub>2</sub> with a cubic shape (Fig. 4c). In the CBD technique, at a certain temperature, the Sn(OH)<sub>4</sub> will attach to the substrate surface during the immersion process, as shown in Fig. 5.

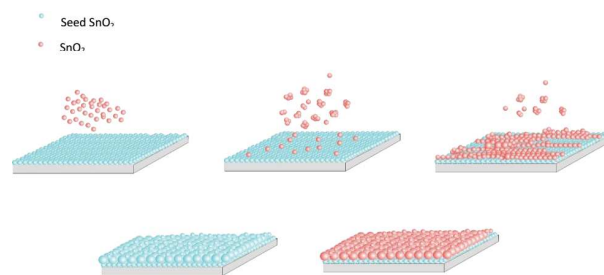


Fig. 5. Illustration of nanostructured SnO<sub>2</sub> thin film growth process by CBD method.

In general, the SnO<sub>2</sub> particles actually have paramagnetic properties and their morphology is affected by the magnetic field. In the case of magnetic field and the HMTA framework-assisted CBD method, the magnetic field not only influences the morphology pattern, but also makes the growth of SnO<sub>2</sub> faster. Therefore, nanostructures of SnO<sub>2</sub> thin films, prepared by magnetic field and HMTA framework-assisted CBD, have a bigger size, compared to those prepared by other methods. The cubic structure of SnO<sub>2</sub> thin film is caused by the framework template of HMTA, that can form three-dimensional pattern of framework in the water solvent. The illustration of the step by step process of the growth of SnO<sub>2</sub> thin films, prepared by magnetic field and HMTA framework assisted CBD, is shown in Fig. 6.

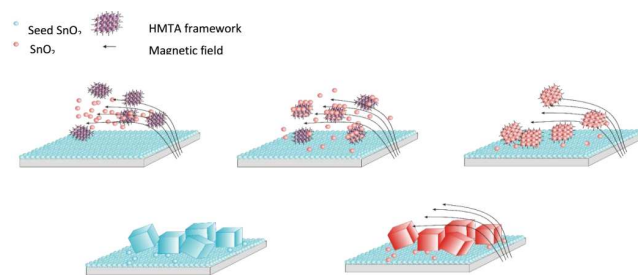


Fig. 6. Illustration of nanostructured SnO<sub>2</sub> thin film growth by magnetic field and HMTA framework assisted CBD method.

The response dynamics of SnO<sub>2</sub> thin film, prepared by the CBD method, with respect to 30 ppm of CO at

RT (300 °C) is shown in Fig. 7a. The pattern of dynamic response from the SnO<sub>2</sub> samples prepared by CBD and samples prepared by magnetic field, and HMTA framework-assisted CBD are similar. In this pattern the response increases as the working temperature increases.

At all temperatures, the response of SnO<sub>2</sub> thin films prepared by CBD is higher than that of SnO<sub>2</sub> thin films prepared by magnetic field and HMTA framework-assisted CBD. This is caused by the differences of their morphology. The big size and cubic shape of SnO<sub>2</sub> may lead to the low specific surface area and a smaller number of adsorption sites, so that the response is lower than that of the nano-spherical-shaped SnO<sub>2</sub> thin film, prepared by CBD.

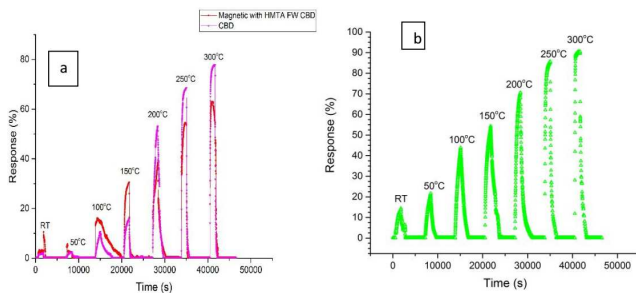


Fig. 7. Response dynamics with respect to 30 ppm of CO gas, for SnO<sub>2</sub> thin film prepared by CBD (a) and by USP (b).

Figure 7b shows the dynamic response of SnO<sub>2</sub> prepared by the USP method, which is higher than that of the SnO<sub>2</sub> thin films prepared by CBD, where the sensor response increases as the working temperature increases. Because of the similar morphology of nanostructured thin films, we can compare the response dynamic of SnO<sub>2</sub> thin films prepared by CBD method and USP method, as shown in Fig. 8.

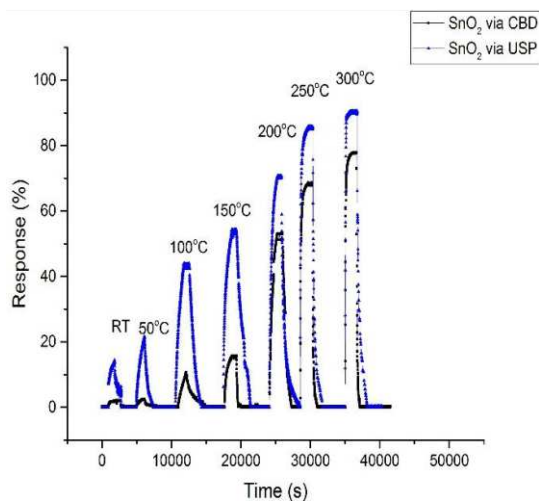


Fig. 8. Response dynamic of SnO<sub>2</sub> thin film prepared by CBD technique, compared to that of SnO<sub>2</sub> thin film prepared by USP.

The sensor response of SnO<sub>2</sub> thin film prepared by USP technique with respect to 30 ppm of CO is higher than the response of SnO<sub>2</sub> thin film prepared by CBD technique. This is because the particle size of SnO<sub>2</sub> thin film prepared by USP is smaller than that prepared by CBD, as was explained earlier. As a result, the specific surface area of SnO<sub>2</sub> prepared by USP will be higher than that of the SnO<sub>2</sub> prepared by CBD.

The CO sensing mechanism can be explained as follows: in the ambient atmosphere, the oxygen, adsorbed on the surface of SnO<sub>2</sub>, takes electrons from the conduction band of SnO<sub>2</sub>, and becomes O<sup>-</sup>. When CO is present, CO adsorbs to the surface, interacts with O<sup>-</sup> to become CO<sub>2</sub>, and releases an electron back to the conduction band, as shown in Eq. 1. This process could change the resistance of SnO<sub>2</sub>, which determines the response.



At higher temperatures, oxygen and CO gas have more energy to be adsorbed on the surface of SnO<sub>2</sub>, so at higher temperatures, more interaction between oxygen ion and CO occurs and thus the response increases with increasing temperature. Figure 9 shows the comparison of CO gas sensor responses at all studied temperatures for all prepared samples. It is clear that the SnO<sub>2</sub> thin films prepared by USP have a higher response at all working temperatures, compared to SnO<sub>2</sub> thin films prepared by other methods.

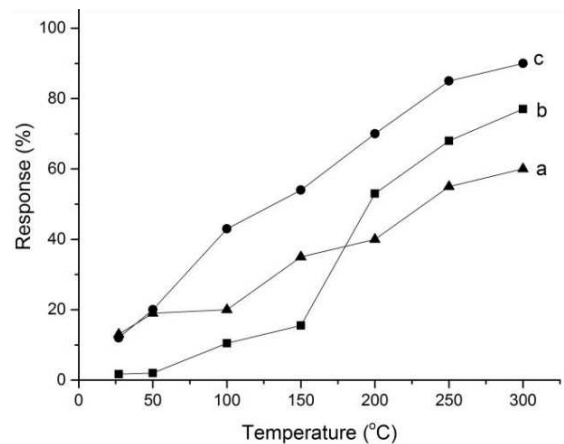


Fig. 9. Response, as a function of working temperature, of SnO<sub>2</sub> thin films prepared by magnetic field and HMTA assisted CBD (a), pure CBD technique (b) and USP technique (c).

#### 4. Conclusions

Morphology modification of SnO<sub>2</sub> nanostructure has been successfully done by ultrasonic spray pyrolysis and the chemical bath deposition method. The morphology of SnO<sub>2</sub> by CBD could be changed by the added effect of a magnetic field and HMTA framework. The resulting SnO<sub>2</sub> morphologies of samples prepared by CBD, magnetic field, HMTA framework-assisted CBD, and USP are spherical, cubic, and spherical, respectively.

The sensor response patterns of nanostructured SnO<sub>2</sub> thin films with respect to 30 ppm of CO, for samples prepared by all tested methods are similar. In these patterns the sensor response increases with the increase of the working temperature. The highest response was obtained with the SnO<sub>2</sub> thin films prepared by USP technique. On the other hand, the SnO<sub>2</sub> thin film sensor reaches the lowest response for the SnO<sub>2</sub> thin film prepared by a magnetic field and HMTA framework-assisted CBD. The difference of responses is greatly influenced by the size and shape of the nanostructure of thin films morphology.

### Acknowledgments

This research has been partially supported by Ministry of Research and Higher Education of Indonesia 2016–2017, and ITB Research Grant 2016–2017.

### References

- [1] L. Wang, Y. Wang, K. Yu, S. Wang, Y. Zhang, C. Wei, *Sensors Actuators B* **232**, 91 (2016).
- [2] S. Li, Y. Li, Y. Wu, W. Chen, Z. Qin, N. Gong, D. Yu, *Phys B: Cond. Mat.* **489**, 33 (2016).
- [3] B. Yulianto, G. Gumilar, N.L.W. Septiani, *Adv. Mater. Sci. Engin.* **2015**, 694823 (2015).
- [4] A.S. Ahmed, M.M. Ahafeeq, M.L. Singla, S. Tabassum, A.H. Naqvi, A. Azam, *J. Luminescence* **131**, 1 (2011).
- [5] T. Tharsika, A.S.M.A. Haseeb, S.A. Akbar, M.F.M. Sabri, *Ceram. Int.* **40**, 5039 (2014).
- [6] A.F. Khan, M. Mehmood, M. Aslam, M. Ashraf, *Appl. Surf. Sci.* **256**, 2252 (2010).
- [7] D. Wei, Y. Shen, M. Li, *J. Nanomater.* **2013**, 761498 (2013).
- [8] V. Bonu, B. Gupta, S. Chandra, A. Das, S. Dhara, A.K. Tyagi, *Electrochem. Acta* **203**, 230 (2016).
- [9] H. Peng, Y. Peng, X. Xu, X. Fang, Y. Liu, J. Cai, X. Wang, *Chinese J. Catalysis* **36**, 2004 (2015).
- [10] L. Fan, X. Li, B. Yon, X. Li, D. Xiong, D. Li, H. Xu, X. Zhang, X. Sun, *Appl. Ener.* **175**, 529 (2016).
- [11] X. Kuang, T. Liu, D. Shi, W. Wang, M. Yang, S. Husain, X. Peng, F. Pan, *Appl. Surface Sci.* **364**, 371 (2016).
- [12] J. Guo, J. Zhang, H. Gong, D. Ju, B. Cao, *Sensors Actuators B* **226**, 266 (2016).